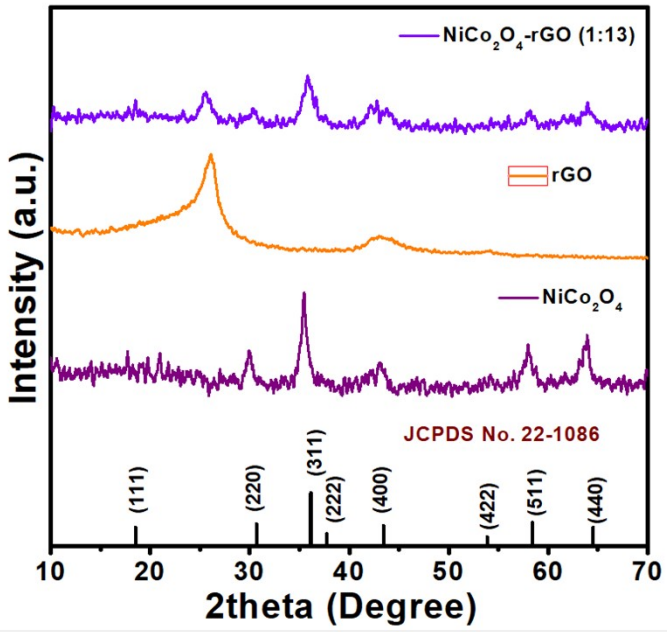

Fig. S1: XRD patterns of $NiCo_2O_4$, rGO and composite of $NiCo_2O_4$-rGO (NCO13).

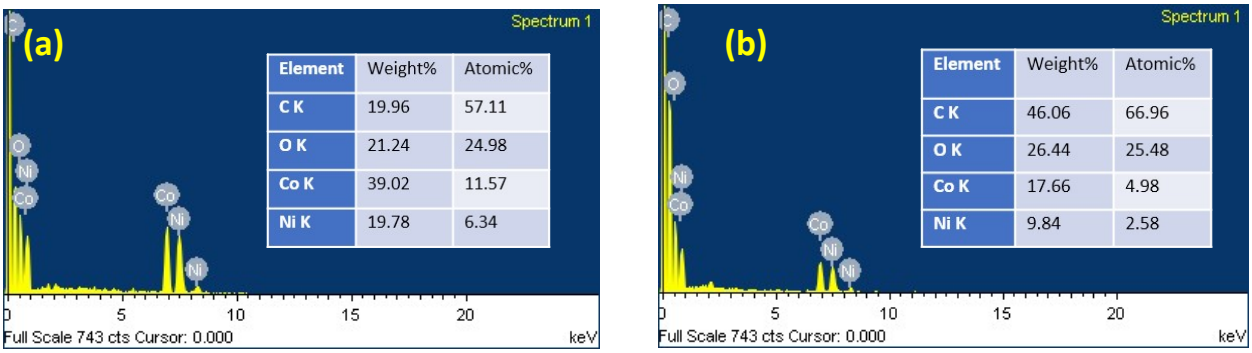

Fig. S2: EDS pattern of (a) NCO13 and (b) NCO26.

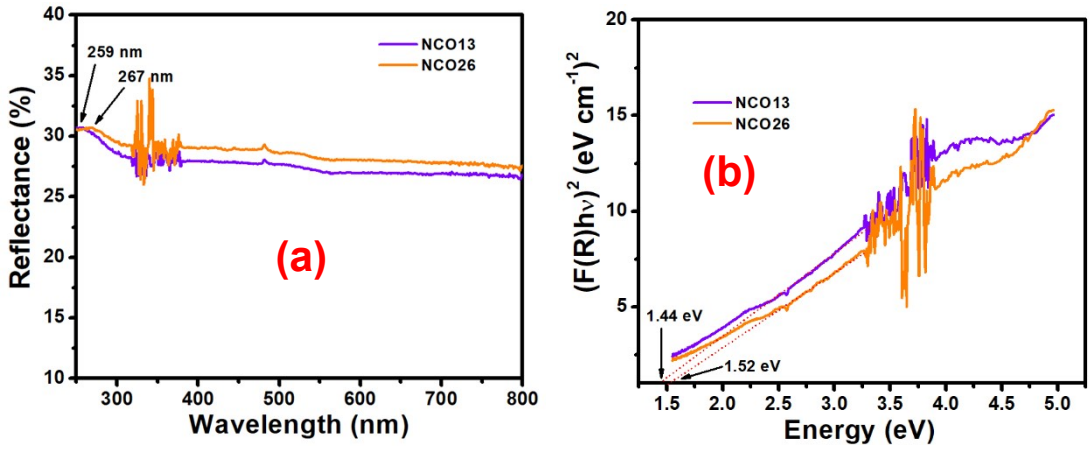

Fig. S3: (a) UV-Vis DRS of NCO13 and NCO26, (b) estimation of band gap energy of NCO13 and NCO26.

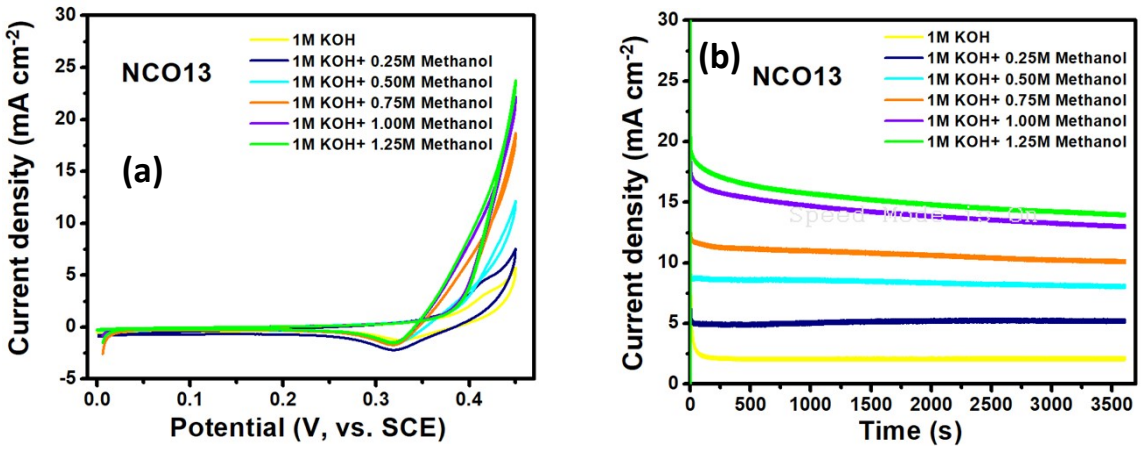

Fig. S4: (a) Cyclic voltammograms of NCO13 towards various concentrations of methanol, (b) Chronoamperograms of NCO towards various concentrations of methanol.

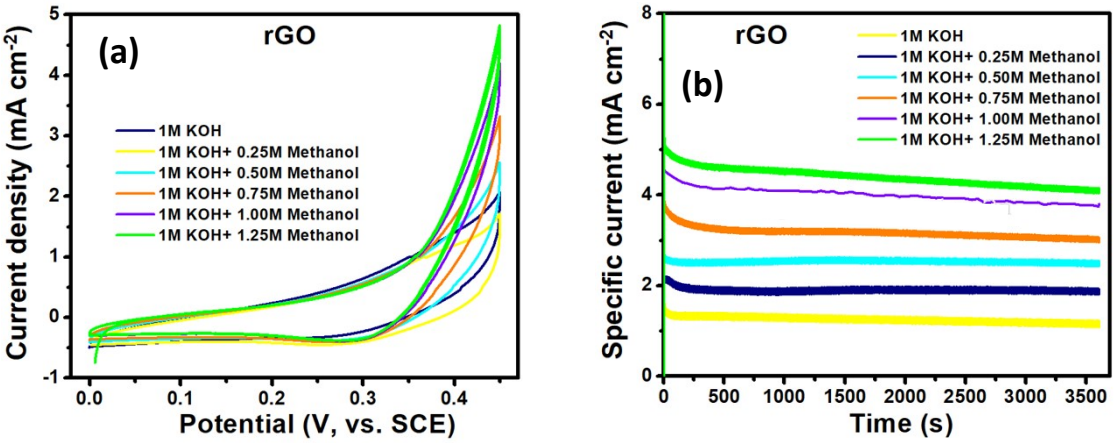

Fig. S5: (a) Cyclic voltammograms of pristine rGO towards various concentrations of methanol, (b) Chronoamperograms of pristine rGO towards various concentrations of methanol.

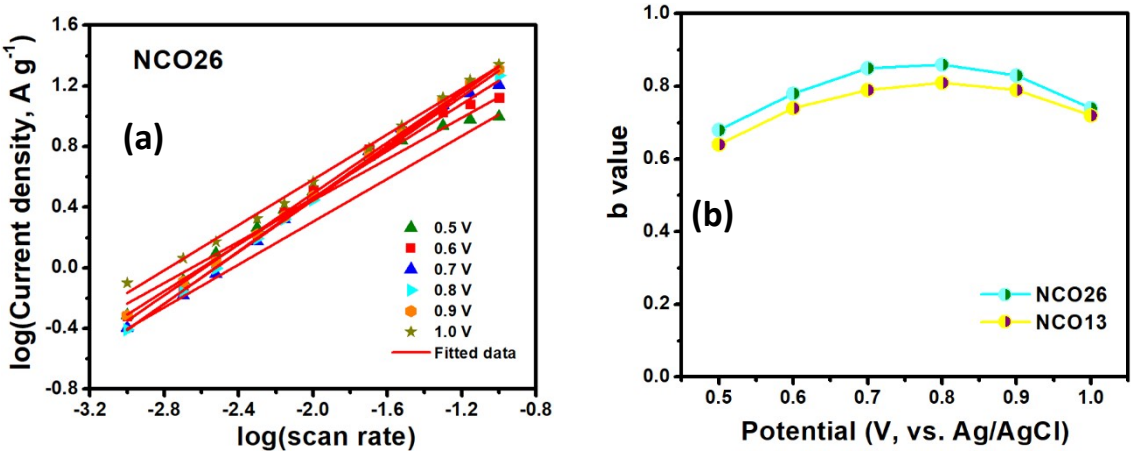

Fig. S6: Plot of log(current density) vs. log(scan rate) for NCO13 (a), plot of b values at various potentials for NCO13 and NCO26 (b).

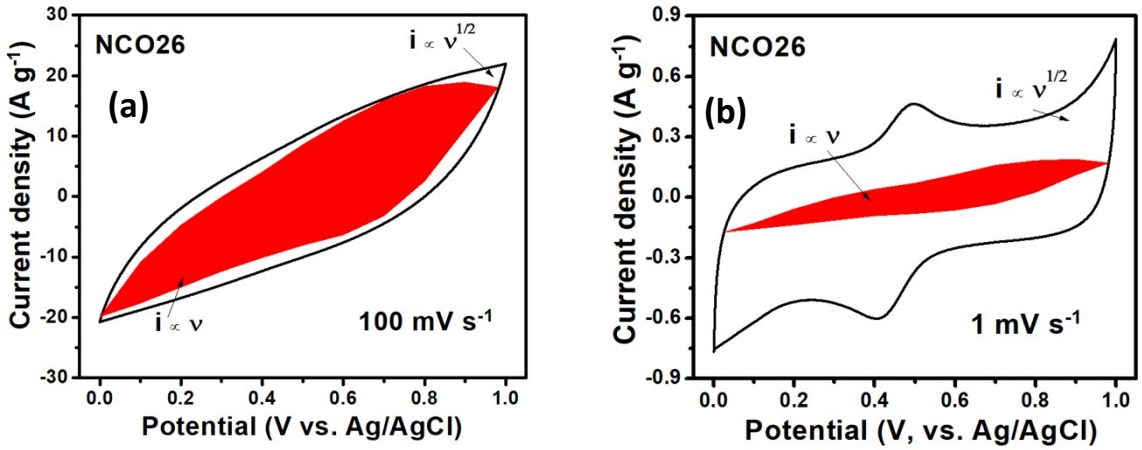

Fig. S7: Cyclic voltammograms showing the capacitive and diffusion-controlled contributions for NCO26 at scan rate of (a) 100 mV s^{-1}, (b) 1 mV s^{-1}.

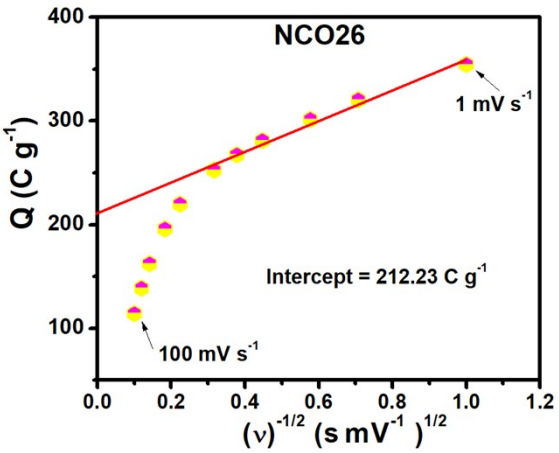

Fig. S8: Plot of Q vs. $\upsilon^{-1/2}$ of NCO 26.

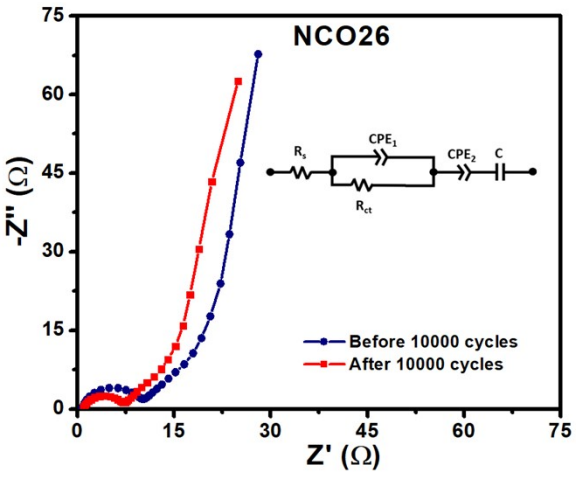

Fig. S9: Nyquist plot of NCO26 before and after 10,000 GCD cycles. Inset shows the fitted electrical equivalent circuit.

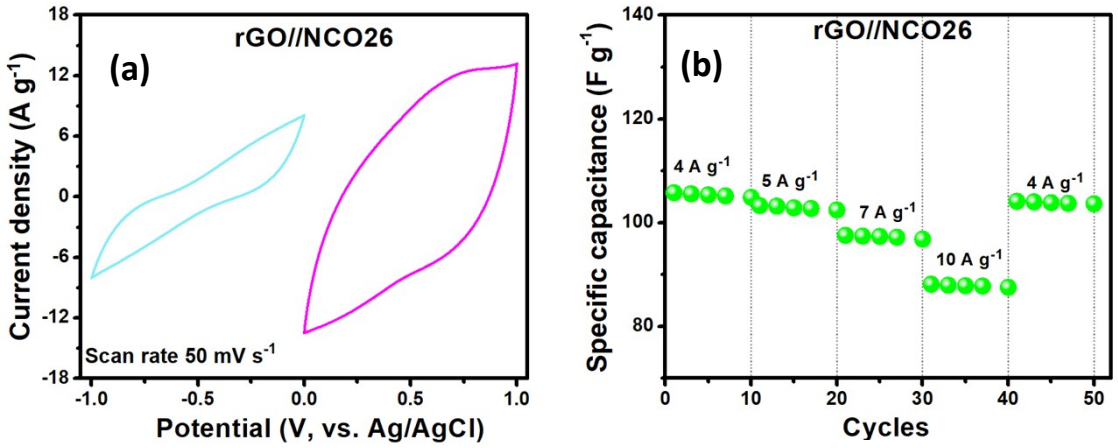

Fig. S10: (a) Cyclic voltammograms of rGO and NCO26 in their respective potential windows. (b) Cycling of supercapacitor device at various current densities.